

2000-GT-0377

## APPLICATION OF MODEL ORDER REDUCTION TO COMPRESSOR AEROELASTIC MODELS

Karen Willcox, Jaime Peraire, and James D. Paduano

Gas Turbine Laboratory  
Department of Aeronautics and Astronautics  
Massachusetts Institute of Technology  
Cambridge, MA 02139

### ABSTRACT

A model order reduction technique that yields low-order models of blade row unsteady aerodynamics is introduced. The technique is applied to linearized unsteady Euler CFD solutions in such a way that the resulting blade row models can be linked to their surroundings through their boundary conditions. The technique is applied to a transonic compressor aeroelastic analysis, in which the high-fidelity CFD forced-response results are better captured than with models that use single-frequency influence coefficients. A low-speed compressor stage is also modeled to demonstrate the multistage capability of the method. These examples demonstrate how model order reduction can be used to systematically improve the versatility, fidelity, and range of applicability of the low-order aerodynamic models typically used for incorporation of CFD results into aeroelastic analyses.

### INTRODUCTION

One of the foremost challenges in the study of free and forced blade vibrations in turbomachinery is encapsulation of aerodynamic effects in a form suitable for coupled aerostructural analysis. It is generally agreed that in modern aeroengines the unsteady aerodynamic effects governing the severity of vibrations are complex; at least some of the flow details (shock motion, blade loading, viscosity, boundary conditions, etc.) must be modeled to obtain realistic analyses. Because very little data exists to isolate the most important of these details, the current state of the art utilizes computational fluid dynamic (CFD) analysis to capture as much of the physics as possible. The CFD results are encapsulated as unsteady aerodynamic forces result-

ing from (usually prescribed sinusoidal) blade vibrations, which can then be coupled to the structural dynamics. Forced vibration analyses are often done in a similar two-step fashion, in which the aerodynamic effects are computed first and then incorporated into a coupled analysis (Chiang and Kielb, 1993). Non-reflecting boundary conditions are commonly used in these analyses for simplicity, although the boundary conditions can have a significant effect on the results (Hall and Silkowski, 1995).

Pre-computation of aerodynamic effects, using canonical motions and forcing functions, invokes various assumptions based on the problem at hand. For stability analysis of a rotor, the fundamental assumption is that the blade vibration frequencies change by only a small amount due to aerodynamic coupling. Thus analysis of the aerodynamic loads using the most important structural dynamic eigenfunctions is justified. Forced vibration analyses often compute gust loads assuming sinusoidal gusts and fixed blades, assuming that the incoming gusts are not modified by unsteady blade motion (Manwaring and Wisler, 1993). Mistuning analyses commonly use simplified aerodynamic models (as in Crawley and Hall (1985)), although incorporation of CFD-based influence coefficients (based on sinusoidal, single-frequency runs) has been reported (Dugundji and Bundas, 1984).

Experience and order-of-magnitude analyses (mass ratio arguments, etc.) suggest that the engineering approximations discussed above are often valid, allowing trends and insight to be more easily obtained. However, the framework for encapsulation of aerodynamic effects is limited, and in some cases inconsistent with the goals of the analysis. Non-sinusoidal forcing, forced response with mistuning, and other analyses that involve combinations of effects stretch the assumptions of standard methods. In

addition, the effects of upstream and downstream boundary conditions (nearby blade rows, inlet duct acoustics) are increasingly coming under scrutiny.

It is in these cases that a reduced-order model with generalized boundary conditions can play an important role. The CFD code is viewed as an input-output model: blade motions, incoming flow perturbations, and mean flow properties are viewed as inputs; outputs include outgoing flow perturbations and the blade forces and moments. A reduced-order model is a low-order model that duplicates the behavior of the CFD analysis over a limited range of conditions. The range of validity of the reduced-order model is determined by the set of CFD experiments performed during the model order reduction procedure. By making the model building procedure systematic, a single tool can yield reduced-order models for a wide range of applications.

In the sense defined above, models based on spatially and temporally sinusoidal motion at a single frequency (we will call these “assumed-frequency” methods) are simple reduced-order models. They are limited to the boundary conditions chosen in the CFD analysis and are only valid at the precise mean flow conditions analyzed. They are limited to a small range of frequencies about the assumed frequency, and this range is unknown. Owing to their limited range of validity, assumed-frequency models are the most compact: they are coupled to the structural model as constant coefficients that are independent of changes in the mean flow, boundary conditions, frequency, etc. More detailed aerodynamic models, motivated by external aeroelastic (wing flutter) methods, have been suggested (Crawley, 1988), but do not appear to be in broad use.

In this paper we present a systematic method for model order reduction from CFD, which can be applied to a broad range of problems. The method allows the analyst to specify the range of interblade phase angles, reduced frequencies, forcing functions, and boundary conditions that are appropriate to encapsulate into the problem at hand. This range is spanned by a series of “canonical” runs of the CFD code, which are then used to derive a low-order model. The model is in ordinary differential equation form, requiring approximately 100 to 200 states per blade row (in our examples), suitable for incorporation in a fully coupled aeroelastic analysis. Examples of application of this model are given for illustrative purposes.

## COMPUTATIONAL MODEL

The starting point for the procedure is a computational model. In this paper, the nonlinear two-dimensional Euler equations, expressed on an unstructured triangular grid, are used:

$$\frac{d\mathbf{U}}{dt} + \mathbf{R}(\mathbf{U}, \mathbf{U}_b, \mathbf{x}) = 0, \quad (1)$$

where  $\mathbf{R}$  represents the nonlinear flux contributions at each node, which are functions of the problem geometry  $\mathbf{x}$ , the unknown

flow quantities on the grid points  $\mathbf{U}$  and the boundary values  $\mathbf{U}_b$ . For a two-dimensional bladed disk with  $r$  blades with rigid cross sections,  $\mathbf{x}$  can be written in terms of plunge displacement  $h_i$  and pitch displacement  $\alpha_i$ :

$$\mathbf{x} = \mathbf{x}(\mathbf{q}), \quad \mathbf{q} = [\mathbf{q}_1^T, \mathbf{q}_2^T, \dots, \mathbf{q}_r^T]^T, \quad (2)$$

where  $\mathbf{q}_i = [h_i \ \alpha_i]^T$ . The vector  $\mathbf{U}_b$  allows external flow disturbances and impedance properties to be modeled. These could be, for example, time-varying pressure or velocity distortions due to a neighboring blade row, inhomogeneity in the incoming flow, or acoustic boundary conditions. Given blade motion  $\mathbf{q}$  and boundary disturbance  $\mathbf{d}$ , we write  $\mathbf{U}_b$  as:

$$\mathbf{U}_b = \mathbf{U}_p(\mathbf{q}, \dot{\mathbf{q}}, \mathbf{d}, \mathbf{x}), \quad (3)$$

where  $\mathbf{U}_p$  is a vector containing the appropriate prescribed quantities.

Linearization of the Euler equations, assuming all motions and disturbances are small, results in the following equation:

$$\frac{d\mathbf{U}'}{dt} + \frac{\partial \mathbf{R}}{\partial \mathbf{U}} \mathbf{U}' + \frac{\partial \mathbf{R}}{\partial \mathbf{U}_b} \mathbf{U}'_b + \frac{\partial \mathbf{R}}{\partial \mathbf{x}} \mathbf{x}' = 0, \quad (4)$$

where prime denotes perturbation quantities, and all partial derivatives are computed at the steady state. Due to the linearity assumption, it is not necessary to actually deform the grid; the final term on the left hand side of equation (4) accounts for the first order effects of grid motion. After linearizing the boundary terms

$$\mathbf{U}'_b = \frac{\partial \mathbf{U}_p}{\partial \mathbf{q}} \mathbf{q}' + \frac{\partial \mathbf{U}_p}{\partial \dot{\mathbf{q}}} \dot{\mathbf{q}}' + \frac{\partial \mathbf{U}_p}{\partial \mathbf{d}} \mathbf{d}' + \frac{\partial \mathbf{U}_p}{\partial \mathbf{x}} \mathbf{x}', \quad (5)$$

and writing the grid displacement as a linearized function of blade displacement  $\mathbf{x}' = \mathbf{T} \mathbf{q}'$ , where the transformation matrix  $\mathbf{T}$  is computed from the mesh geometry, we obtain a high-order state space system for the perturbation quantities

$$\frac{d\mathbf{U}'}{dt} + \frac{\partial \mathbf{R}}{\partial \mathbf{U}} \mathbf{U}' = \left[ -\frac{\partial \mathbf{R}}{\partial \mathbf{x}} \mathbf{T} - \frac{\partial \mathbf{R}}{\partial \mathbf{U}_b} \left( \frac{\partial \mathbf{U}_p}{\partial \mathbf{q}} + \frac{\partial \mathbf{U}_p}{\partial \mathbf{x}} \mathbf{T} \right) \right] \mathbf{q}' - \frac{\partial \mathbf{R}}{\partial \mathbf{U}_b} \frac{\partial \mathbf{U}_p}{\partial \dot{\mathbf{q}}} \dot{\mathbf{q}}' - \frac{\partial \mathbf{R}}{\partial \mathbf{U}_b} \frac{\partial \mathbf{U}_p}{\partial \mathbf{d}} \mathbf{d}' \quad (6)$$

which can be written equivalently as

$$\frac{d\mathbf{U}'}{dt} = \mathbf{A} \mathbf{U}' + \mathbf{B} \mathbf{u} + \mathbf{E} \mathbf{d}. \quad (7)$$

Here  $\mathbf{u} = [\mathbf{q} \ \dot{\mathbf{q}}]^T$  is the input vector containing the displacement and velocity of each blade, and the matrices  $B$  and  $E$  contain the appropriate forcing terms from equation (6).

To determine the unsteady response of the cascade, the inputs  $\mathbf{u}(t)$  and  $\mathbf{d}(t)$  are specified and the large system (7) is time-marched to determine the resulting flow. Often we are interested not in the flow itself, but in relevant output quantities. These are typically the forces and moments acting on the blades, but could be any feature of the response. We define an output vector  $\mathbf{y}$  as

$$\mathbf{y} = C\mathbf{U}', \quad (8)$$

which for the analyses presented here contains the aerodynamic force and moment acting on each blade and the outgoing flow perturbations.  $C$  is a matrix containing the linearized force calculation.

The system of ordinary differential equations (7, 8) can be coupled into an aeroelastic model, since the input  $\mathbf{u}$  and output  $\mathbf{y}$  can be directly linked to a structural model. However, equation (7) has tens of thousands of states per blade passage (four unknowns for every point on the computational domain). Suitable models for aeroelastic analyses must have a much lower number of states, and can be derived using systematic model order reduction procedures. Such techniques are introduced in the next section.

## MODEL ORDER REDUCTION PROCEDURE

Reducing the order of a system such as (7,8) is a problem which has been studied in great detail in various contexts (Dowell et al., 1999). Many procedures are not suitable for the problem at hand, however, because they require computation of the eigenvalues and eigenvectors of  $A$ ; this is not practical for the problem sizes of interest in turbomachinery aeroelasticity. In addition, such approaches do not extend to nonlinear systems. Other methods, such as the proper orthogonal decomposition (POD), rely on robust computational procedures. These “projection” methods follow the following basic steps:

- Compute a small number of solutions using the full model. The conditions for these full solutions or “snapshots” are chosen to span the operating range over which fidelity to the CFD results is desired.
- Create a set of basis vectors which capture the behavior in the solutions. “Behavior” can be quantified by spatial patterns in the flow, snapshots of the unsteady response (frequency domain), or the input-output transfer functions. The number of basis vectors required depends on the problem and the desired degree of fit.
- Project the original equations onto the space represented by the basis vectors. The result is a set of ordinary differential equations (ODEs) for the time-varying coefficients of the

basis vectors. The low-order system is completely defined by these coefficients or “states”; approximate reconstruction of the entire flow field can be accomplished by multiplying the states by the basis vectors. Thus any output quantity (blade pressure distribution, downstream disturbances, forces and moments) can be approximated.

This procedure has been developed and reported on in previous work. In Willcox et al. (1999a), a unique application of the POD method for linearized systems is described, which uses frequency domain instead of time domain solutions to create a low-order model. In Willcox et al. (1999b), a similar method based on Arnoldi vectors, and their connection with the POD, is discussed. Appendix A outlines how the above steps are accomplished using these two methods. The ODEs for the reduced-order model are written

$$\dot{\mathbf{v}} = A\mathbf{v} + B\mathbf{u} + E\mathbf{d} \quad (9)$$

$$\mathbf{y} = C\mathbf{v} \quad (10)$$

where the states in  $\mathbf{v}$  are akin to generalized coordinates, being the amplitudes of the individual basis vectors.

Using these projection methods, a model of the form (9, 10) can be obtained for an entire blade row. In Willcox (2000), it is shown that each interblade phase angle can typically be represented over a broad frequency range using 6 to 10 states. Thus for a full blade row analysis, model orders of 100-500 states are required, depending on the number of blades and the frequency range of interest. This represents a three order of magnitude reduction in model order from the full model, allowing many coupled aero-structural and aero-acoustic analyses that would otherwise be impossible. Here, results are presented for two-dimensional, inviscid flow, although the model order reduction methodology is applicable to any linearized CFD model.

## EXAMPLES

In this section the model order reduction procedure is applied, and compared to the results obtained by applying assumed-frequency methods to the same problems. The intent is to show the qualitative differences between the methods for relevant examples, rather than to draw quantitative conclusions. All plotted quantities represent non-dimensional parameters. In the ensuing results, lengths have been non-dimensionalized by the rotor chord length, and velocities by the ambient speeds of sound. Thus non-dimensional frequency  $\omega$  is related to reduced frequency  $k$  by  $\omega = kM$ , where  $M$  is the inlet Mach number.

### Test Cases

**Transonic Rotor** A transonic fan blade design is used in our first two examples. Figure 1 shows the airfoil chosen for

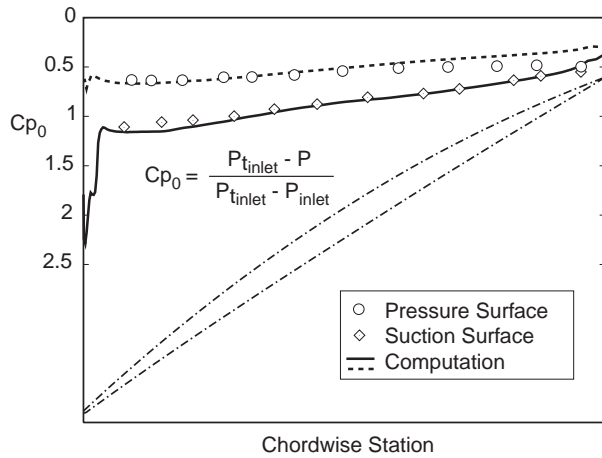


Figure 1. DFVLR transonic rotor from Youngren (1991), and steady pressure coefficient profile computation compared to data from Schreiber and Starken (1984).

our test cases (Youngren, 1991), together with a comparison of the steady pressure distribution to data (Schreiber and Starken, 1984). The test conditions are inlet Mach number 0.82, relative flow angle  $58.5^\circ$ , blade angle  $49^\circ$ , and ambient sea level pressure and temperature. The structural system consists of 20 blades each with a mass ratio of 100, decoupled bending and twist motion, and a first bending (plunge motion) reduced frequency referenced to the chord of 0.12.

**Low-Speed Stage** For our third example, a low-speed compressor stage is analyzed. The airfoil coordinates represent the third stage of a four-stage low-speed research compressor described in Silkowski (1995). The test conditions are inlet Mach numbers of 0.165 and 0.123, and inlet flow angles of  $59.3^\circ$  and  $47.3^\circ$  in the rotor and stator respectively. The gap between the stator and rotor is 47.5% of the rotor chord. Both the rotor and stator are analyzed, assuming that the rotor has 16 blades and the stator has 20 (the actual compressor stage has 54 rotor blades and 74 stator vanes, but a smaller problem was chosen to simplify the analysis). One quarter of the periodic domain (containing five stator blades and four rotor blades) is shown in Figure 2, although for generality, the analysis is carried out on the full stage.

### Example 1: Frequency Dependence of Aerodynamic Response Coefficients

To illustrate how the low-order model captures the aerodynamic response to blade motion, a series of CFD solutions near the blade bending frequency  $\omega = 0.1$  ( $k = 0.12$ ) for the transonic rotor test case were obtained. These snapshots were taken for each interblade phase angle at zero frequency and at 90, 95, 100, 105, 110, 150 and 200 percent of the blade structural frequency.

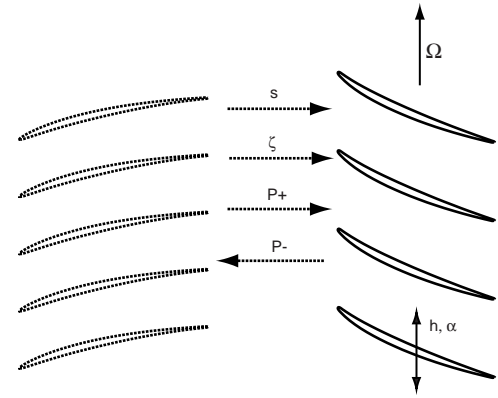


Figure 2. Low-speed airfoil cross-sections from Silkowski (1995), shown for one quarter of the computational domain used for stage analysis. Arrows represent the characteristic waves: entropy wave ( $s$ ), vorticity wave ( $\zeta$ ) and downstream and upstream running pressure waves ( $P+$  and  $P-$ ).

This resulted in 16 snapshots of the frequency-domain response of the system per interblade phase angle (8 frequencies  $\times$  2 snapshots per frequency - real and imaginary parts). The boundary conditions for these CFD trials were non-reflecting, but the procedure yields models suitable for coupling to other blade rows.

Unsteady aerodynamic lift forces on the blade were computed for each interblade phase angle, using both the CFD results and reduced-order models. Figure 3 shows the results for interblade phase angles of  $90^\circ$ ,  $180^\circ$  and  $270^\circ$  degrees. Both the  $90^\circ$  and the  $180^\circ$  cases show a linear variation in forced response amplitude, with almost no phase variation. It was determined that by retaining the first four POD modes computed from the available 16 snapshots, both the phase and the magnitude of the response could be accurately captured over the entire sample range (an exact match would be obtained if all 16 snapshots were used, but the resulting model order would be unnecessarily high). The dynamics for the  $270^\circ$  degree mode are more complicated, with a local resonance present near a frequency of 0.14. In this case, by choosing the snapshots at zero frequency and at  $\omega=0.15$ , the phase and magnitude can be (fairly accurately) captured using a second order model.

At interblade phase angles of  $90^\circ$  and  $180^\circ$ , the blade unsteady forces are not strongly dependent on reduced frequency. In the range of reduced frequencies from 0.09 to 0.11, an assumed-frequency method would introduce an error of about 10% in unsteady forcing. However, at an interblade phase angle of  $270^\circ$ , there is strong frequency dependence. Using the unsteady force calculated at  $\omega = 0.1$  would introduce an error of 36% at 0.09 and 30% at 0.11. The reduced-order model, on the other hand, tracks this strong variation of blade force magnitude. At 0.09 the reduced-order model error is 9%, at 0.1 it is 12%, and at 0.11 it is 18%. Thus the model trades fidelity at the assumed frequency for better reproduction of the CFD results over a broad range of frequencies, at the expense of additional computations. One could further improve the accuracy by incorporating

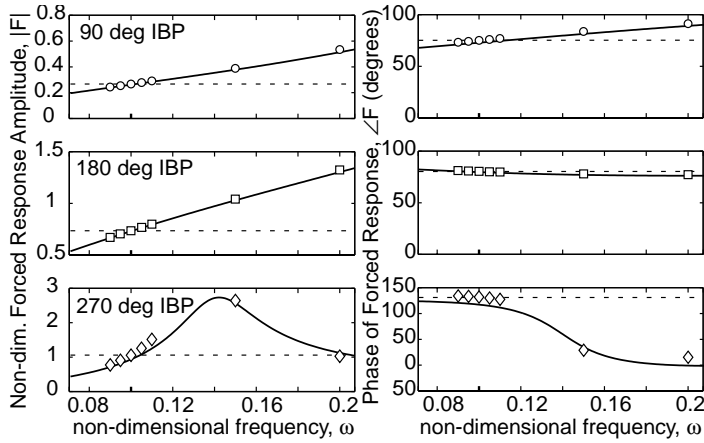


Figure 3. Unsteady aerodynamic plunge force on the DFVLR transonic rotor, computed at several reduced frequencies (symbols) and plotted against reduced-order model results (solid lines). Dashed lines show assumed frequency predictions, which are constant with frequency.

additional POD modes in the reduced-order model. This would require no additional snapshot computations, but would make the resulting model order higher.

As the range of frequencies of interest broadens further, the disparity between the two models becomes more severe. Figure 3 shows that the low-order model faithfully reproduces the CFD force results over the entire range of interblade phase angles and frequencies it is designed to model.

## Example 2: Forced Response Comparisons

The low-order model from the previous analysis can be coupled to a structural model, to determine the effect of aerodynamics on system stability and forced response. Such calculations can be compared to those computed using an assumed frequency for both the forcing function and the blade motion.

To create a coupled system, the structural dynamics are first represented by a system of ODEs forced by aerodynamic blade forces  $\mathbf{y}$  (from the aerodynamic model), whose states/outputs are the blade displacements and motions  $\mathbf{u}$ :

$$\dot{\mathbf{u}} = \mathbf{S}\mathbf{u} + \mathbf{T}\mathbf{y}. \quad (11)$$

This structural model is then coupled to the aerodynamic reduced-order state-space system (9,10). The coupled system is as follows:

$$\begin{bmatrix} \dot{\mathbf{v}} \\ \dot{\mathbf{u}} \end{bmatrix} = \begin{bmatrix} \mathbf{A} & \mathbf{B} \\ \mathbf{T}\mathbf{C} & \mathbf{S} \end{bmatrix} \cdot \begin{bmatrix} \mathbf{v} \\ \mathbf{u} \end{bmatrix} + \begin{bmatrix} \mathbf{E} \\ \mathbf{0} \end{bmatrix} \cdot \mathbf{d}. \quad (12)$$

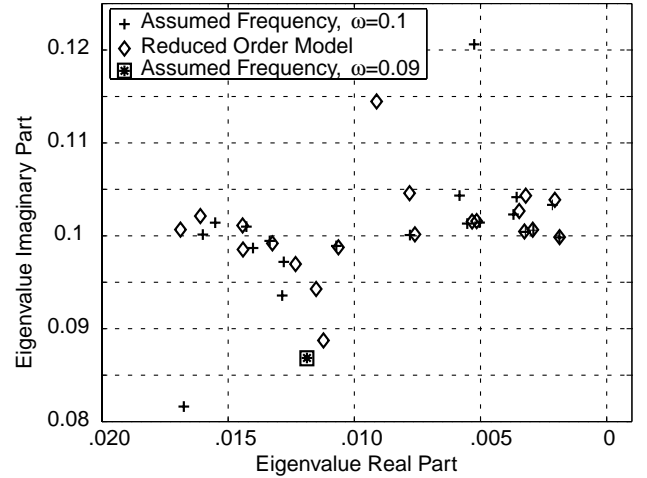


Figure 4. Comparison of eigenvalues obtained using reduced-order model and assumed-frequency method.

Note that the coupling of the low-order model to the upstream and downstream flowfields is not explicitly shown in this equation. If the perturbation flow inputs at the boundaries are assumed to be zero or are prescribed (for forced response analysis), and the perturbation flow outputs are not allowed to excite any external dynamical systems (such as duct acoustics), the system is uncoupled to the upstream and downstream flowfields, i.e. the boundaries are non-reflecting.

The eigenvalues of this system can be compared to those computed using aerodynamic influence coefficients computed at the blade natural frequency of  $\omega = 0.1$ . Figures 4 and 5 show that both methods yield similar eigenvalues over a broad range of interblade phase angles, but in the critical region near a nodal diameter of 15, the methods differ by 10% in frequency and 50% in damping. For a mode with  $\ell$  nodal diameters, the corresponding interblade phase angle is  $\sigma = 2\pi\ell/r$ , where  $r$  is the number of blades (in this example  $r = 20$ ). The mode  $\ell = 15$  therefore corresponds to an interblade phase angle of  $270^\circ$ . To show that the reduced-order model yields higher fidelity results, the influence coefficients are recomputed at  $\omega = 0.09$ , and the resulting eigenvalues are also shown in Figure 5. Note that the eigenvalue at  $\ell = 15$ , whose frequency is about 0.09, matches that predicted by the low-order model (this is also shown in Figure 4), and the eigenvalue at  $\ell = 16$  is more poorly predicted than in either of the previous calculations.

The effect of the change in eigenvalues on the forced response behavior is shown in Figure 6. To obtain these results using the assumed-frequency method, influence coefficients must be computed for the specific forcing function being modeled. A sinusoidal axial velocity defect with 15 nodal diameters ( $\sigma = 270^\circ$ ), rotating at a non-dimensional frequency  $\omega = 0.1$ , was applied in the CFD code, assuming no blade motion. The CFD results were incorporated into the assumed-frequency model, resulting in a model that assumes both the temporal and spatial fre-

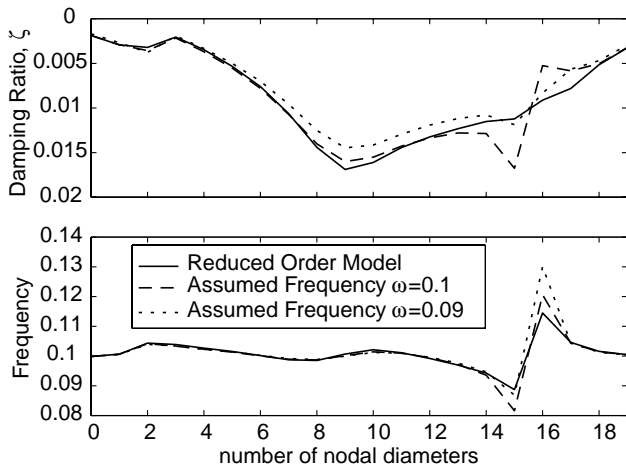


Figure 5. Comparison of damping and frequency of eigenvalues obtained using reduced-order model and assumed-frequency method.

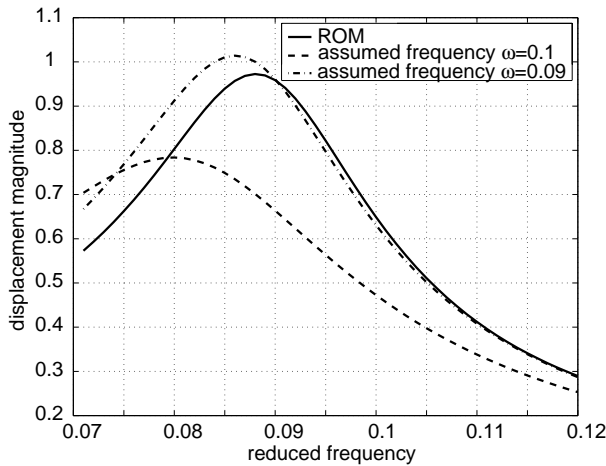


Figure 6. Displacement response of the transonic rotor to excitation over a broad range of reduced frequencies.

quency of the excitation. Both models were then excited at the same nodal diameter over a range of temporal frequencies. The resulting blade displacement predictions illustrate the inaccuracies that result from assuming the temporal forcing frequency; similar inaccuracies result from assuming the nodal diameter and spatial shape (sinusoidal) of the forcing.

Figure 6 shows that the assumed-frequency method introduces error in two ways. First, because it underpredicts the frequency of the coupled system eigenvalue, the peak forced response is at a lower frequency than the actual peak. The response of the coupled system at the forcing frequency is thus underpredicted. Second, because the damping ratio is overpredicted, the overall response is less severe. The combined effect is a 26% underprediction of the forced response at  $\omega = 0.1$  when compared to the reduced-order model. The peak response of the system

is underpredicted by about 20%. Our conjecture is that the errors introduced by the assumed-frequency method would be even higher for lower system damping ratio, because the frequency peaks would be narrower and more sensitive to small changes in damping ratio.

To show that the reduced-order model results are correct, the aerodynamic influence coefficients were recomputed at an assumed frequency of 0.09, which is much closer to the actual eigenvalue frequency for the fifteenth nodal diameter mode. The computed forced response is very close to that computed by the reduced-order model, and the eigenvalue for the fifteenth nodal diameter mode is much closer to that predicted by the reduced-order model as shown by the asterisk on Figure 4. Note that applying the assumed-frequency method iteratively would probably yield the correct answer, but would require at least two additional iterations if the reduced-order model information were not available. We avoid the iterative procedure by encapsulating several CFD runs into one low-order model. Similarly, determining the effect of various non-sinusoidal forcing functions is cumbersome using assumed-frequency methods, but straightforward using reduced-order models.

### Example 3 - Multistage Analysis

Our model order reduction procedure incorporates two important features - a model whose complexity is consistent with a user-specified range of validity, and a structure that allows blade rows to be coupled to their surroundings. To illustrate how these two features are exercised in a multi-stage analysis, this example analyzes a low-speed compressor stage, comparing the stability and response properties of a rotor before and after the inclusion of an upstream stator row.

Our example is the low-speed compressor stage described at the beginning of this section, which has a non-dimensional period of  $T = 316$  for one rotor revolution. Because the Mach number of this example is low, the system's actual reduced frequency is quite high; for this example we choose a lower reduced frequency ( $k = 0.5$ ) to increase the interaction between the structural dynamics and aerodynamics.

To create a multistage model, the rotating and stationary blade rows must be coupled. To accomplish this, reduced-order models for each blade row are first developed in the relative reference frame using the Arnoldi-based approach (see Appendix A). The models are then coupled in a time-marching simulation by moving the grids at each time step. The generalized boundary conditions in the reduced-order models for each blade row allow them to communicate as shown in Figure 2. The resulting system is time varying because of the relative motion of the blade rows.

To look at the blade force during transients, a time marching simulation is performed with no coupling of the aerodynamic force to the structure. The first blade of the compressor is prescribed to execute a pulse-like plunging motion, which excites all reduced frequencies  $k < 11$  (see Willcox (2000) for details).

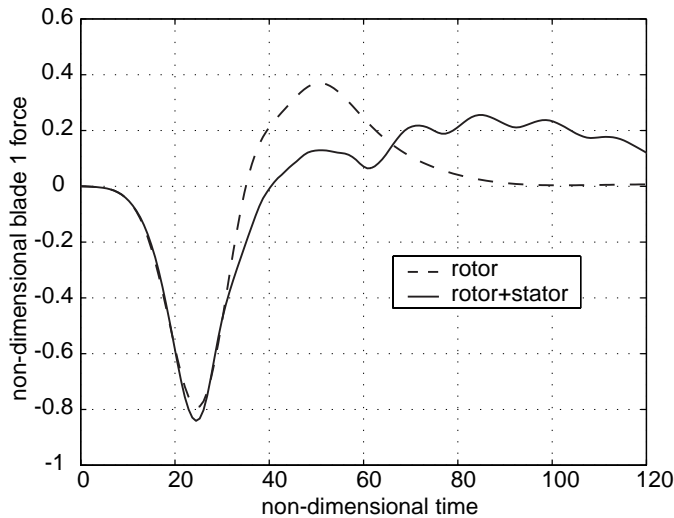


Figure 7. Aerodynamic force on blade 1 of the low-speed rotor due to a prescribed pulse input on its plunge displacement. Blades are considered rigid for this run.

The resulting aerodynamic plunge force on the blade is plotted in Figure 7 for the rotor-only and the rotor-stator case. In the rotor-only case, the pulse input results in an initial plunging force on the blade. Subsequent to this, there is a reaction force due to the impedance of the overall fluid system, which persists for approximately 0.3 rotor revolutions. When the stator is coupled to the system, the picture changes in two ways. First, a periodic force is superimposed on the basic response, whose frequency corresponds to the blade passing frequency between the stages. Second, the response of the system is sustained over a much longer period of time, indicating that the phase properties of the fluid dynamic system have changed.

The blade forces are next examined for the coupled aero-structural system. Figure 8 shows the coupled system's response when the first blade is given an initial deflection, and the system is allowed to "ring down" over multiple rotor revolutions. The initial condition excites all interblade phase angles simultaneously, so the response will evolve toward the least stable interblade phase angle as time proceeds. The decaying oscillations that exist for the rotor only become sustained oscillations when the stator is added, with superimposed high frequency forces due to the stator passing.

Although the system we have created is time varying, so that linear time invariant analyses are not strictly valid, a crude stability analysis can be performed by computing the frozen-time eigenvalues over the range of relative positions of the blade rows. Figure 9 shows the eigenvalues computed in this way, comparing the rotor-only eigenvalues and the eigenvalues for the stage with a stator-rotor gap of 47.5% of the rotor chord. Note that the rotor-stator eigenvalues appear in closely packed clusters, indicating that the system is only weakly time-varying. All of the eigenvalue clusters lie entirely in either the left or right half plane, so

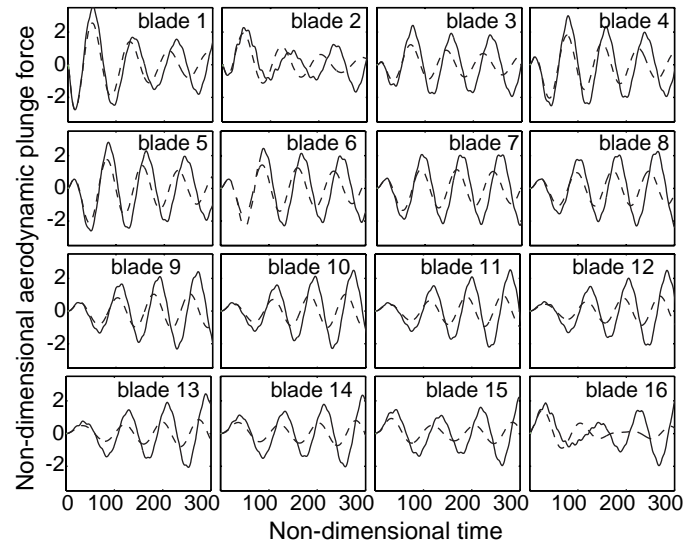


Figure 8. Force on every blade of low-speed rotor due to an initial displacement of the coupled system. The structure and aerodynamics are coupled in this run. Solid - with stator, dashed - no stator.

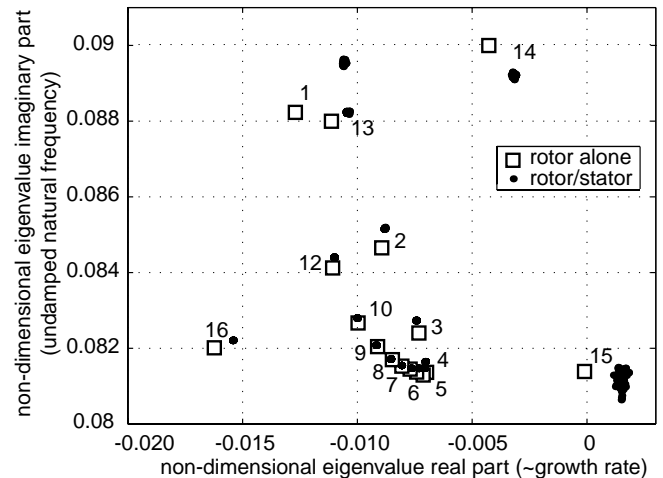


Figure 9. Eigenvalues of the low-speed rotor. Eigenvalues are numbered by their nodal diameter ( $\sigma = 2\pi\ell/16$ ).

stability of the system is assumed to depend on the locations of these clusters. Based on this assumption, Figure 9 indicates that the eigenvalues associated with a nodal diameter of  $\ell = 15$  (interblade phase angle of  $337.5^\circ$ ) are destabilized by bringing the stator into the proximity of the rotor. This explains the difference between the responses in Figure 8.

## DISCUSSION AND CONCLUSIONS

Because the models created using projection methods are much lower order than their CFD counterparts, modeling the be-

behavior of entire compressors is feasible. Such modeling must be done with a clear goal in mind, so that the appropriate range of validity is built in to the reduced-order models. But because the procedure is systematic, and because the low-order models allow interconnection of upstream and downstream impedance conditions, one can envision a design system that allows many types of interactions to be studied using the same baseline codes.

In the examples presented in this paper, we showed potential areas where such a design system would allow higher fidelity, more complete aeroelastic analysis to be carried out. The fact that the solutions obtained using reduced-order models capture the CFD results better than those obtained with simpler models is not surprising: more detailed information is computed and incorporated, yielding improved results in a direct way.

While derivation of models using the POD technique will in general be as expensive as an assumed-frequency approach, the Arnoldi method can be used efficiently to derive high-fidelity reduced-order models. For example, with  $r$  blades, we require just  $r$  matrix factorizations to obtain the Arnoldi reduced-order model. The assumed-frequency method will require  $r$  factorizations per frequency iteration, while the POD requires  $r$  factorizations per snapshot frequency. To obtain an accurate model, the number of snapshot frequencies will be comparable to (or may exceed) the number of frequency iterations one might use to obtain the desired fidelity using an assumed-frequency approach. Clearly, the Arnoldi method is more desirable; however it is a new approach and has not yet been implemented for all types of problems. Hence we have obtained some of the results here using the more expensive POD. For a more complete comparison of POD and Arnoldi methods, see Willcox et al. (1999b).

Using either the POD or Arnoldi approach, the resulting models are valid over a (chosen) range of frequencies for general forcing inputs. Methods that assume both the shape and frequency of motion and forcing have unknown, potentially small ranges of validity. In contrast, reduced-order models can be used over the appropriate frequency range with the confidence of the original high-fidelity CFD code. Whether the improvements obtained are worth the computational effort remains to be determined, and will depend on the specific problem considered. Therefore the question of whether reduced-order models are necessary and cost-effective is not addressed here; we have instead demonstrated the following:

- Model order reduction can be applied in a generalized framework that is independent of the CFD code used. This capability is achieved through the use of canonical snapshots of the flow, rather than eigenvalue analyses or methods involving frequency domain fitting. Using this framework, application of reduced-order modeling to a turbomachinery Euler code was demonstrated for the first time.
- A variety of problems can be studied using reduced-order modeling, provided that the range of desired model validity

is carefully defined. In particular, analyses involving multiple simultaneous effects, broadband temporal/spatial excitation, or multiple stages are feasible.

- Because of their matrix ordinary differential equation form (also known as “state space” form), reduced-order models can be easily introduced into existing aeroelastic analyses. This allows one to assess the impact of assumed-frequency models on fidelity, and easily incorporate additional computational results into the analysis when warranted.

- Initial results using realistic blade rows indicate that the fidelity of existing aeroelastic methods may in fact be insufficient, especially if the blade row is assumed to be isolated. Further research is required in this area.

## ACKNOWLEDGMENTS

The authors would like to thank Asif Khalak for his comments and conceptual contributions. This research was supported by AFOSR Grant #F49620-95-1-0409, Marc Jacobs, technical monitor.

## REFERENCES

- Berkooz G., Holmes P., and Lumley J., 1993. “The Proper Orthogonal Decomposition in the Analysis of Turbulent Flows.” *Annual Review of Fluid Mechanics*, vol. 25 pp. 539–575.
- Chiang H.D. and Kielb R.E., 1993. “An Analysis System for Blade Forced Response.” *Journal of Turbomachinery*, vol. 115, 4 pp. 762–770.
- Crawley E., 1988. “Aeroelastic Formulation for Tuned and Mistuned Rotors.” AGARD Manual on Aeroelasticity in Axial-Flow Turbomachines Volume 2.
- Crawley E. and Hall K., 1985. “Optimization and Mechanisms of Mistuning in Cascades.” *Engineering For Gas Turbines and Power*, vol. 107 pp. 418–426.
- Dowell E., Hall K., Thomas J., Florea R., Epureanu B., and Heeg J., 1999. “Reduced Order Models in Unsteady Aerodynamics.” AIAA 99-1261.
- Dugundji J. and Bunas D., 1984. “Flutter and Forced Response of Mistuned Rotors Using Standing Wave Analysis.” *AIAA Journal*, vol. 22, 11 pp. 1652–1661.
- Feldmann P. and Freund R., 1995. “Efficient Linear Circuit Analysis by Padé Approximation via the Lanczos Process.” *IEEE Transactions on Computer-Aided Design of Integrated Circuits and Systems*, vol. 14 pp. 639–649.
- Grimme E., 1997. *Krylov Projection Methods for Model Reduction*. Ph.D. thesis, Coordinated-Science Laboratory, University of Illinois at Urbana-Champaign.
- Hall K. and Silkowski P., 1995. “The Influence of Neighboring Blade Rows on the Unsteady Aerodynamic Response of Cascades.” ASME 95-GT-35.

Manwaring S.R. and Wisler D.C., 1993. "Unsteady Aerodynamics and Gust Response in Compressors and Turbines." *Journal of Turbomachinery*, vol. 115, 4 pp. 724–740.

Romanowski M. and Dowell E., 1994. "Using Eigenmodes to Form an Efficient Euler Based Unsteady Aerodynamics Analysis." Proceedings of the Special Symposium on Aeroelasticity and Fluid/Structure Interaction Problems, ASME International Mechanical Engineering Congress and Exposition, AD-Vol. 44, pp. 147-160.

Schreiber H. and Starke H., 1984. "Experimental investigation of a transonic compressor rotor blade section." *Journal of Engineering for Gas Turbines and Power*, vol. 106 pp. 288–294.

Silkowski P., 1995. "Measurements of Rotor Stalling in a Matched and Mismatched Compressor." GTL Report 221, MIT.

Sirovich L., 1987. "Turbulence and the Dynamics of Coherent Structures. Part 1 : Coherent Structures." *Quarterly of Applied Mathematics*, vol. 45, 3 pp. 561–571.

Willcox K., Paduano J., Peraire J., and Hall K., 1999a. "Low Order Aerodynamic Models for Aeroelastic Control of Turbo-machines." AIAA 99-1467.

Willcox K., Peraire J., and White J., 1999b. "An Arnoldi Approach for Generation of Reduced-Order Models for Turbo-machinery." Submitted, *Computers and Fluids*.

Willcox K.E., 2000. *Reduced-Order Aerodynamic Models for Aeroelastic Control of Turbomachines*. Ph.D. thesis, Dept. of Aeronautics and Astronautics, MIT.

Youngren H., 1991. *Analysis and Design of Transonic Cascades with Splitter Vanes*. Master's thesis, Dept. of Aeronautics and Astronautics, MIT.

## Appendix A

Some details of the steps outlined in the discussion of model order reduction procedures are given in this appendix. For further details, see Willcox (2000).

### Generation of snapshots

Typically, projection methods for model order reductions begin with *snapshots* of the flow field obtained from a time-marching simulation. This is impractical for an entire bladed disk, and unnecessary for linearized flows. A more efficient approach is to decompose the forcing and aerodynamic response into spatial and temporal Fourier modes, as is typical in aeroelastic analysis. Blade motion is decomposed into  $r$  discrete spatial Fourier modes with interblade phase angles  $\sigma_j = \frac{2\pi j}{r}$ , where  $r$  is the number of blades in the compressor, and an infinity of temporal frequencies  $\omega_k$ . External disturbance forcing is similarly viewed as a summation over an infinite number of spatial and temporal modes with frequencies  $\sigma_j$  (now for any  $j$  since the disturbance is a continuous function) and  $\omega_k$  respectively. Blade

motion  $\mathbf{u}$  and disturbances  $\mathbf{d}$  are thus written for any blade passage  $n$  as follows:

$$\mathbf{u}_n^{jk}(t) = \tilde{\mathbf{u}}_{jk} e^{i\omega_k t} e^{i(n-1)\sigma_j} \quad (13)$$

$$\mathbf{d}_n^{jk}(b, t) = \tilde{\mathbf{d}}_{jk} e^{i\omega_k t} e^{i(n-1)\sigma_j} \quad (14)$$

where  $b$  denotes the boundary along which  $\mathbf{d}$  is defined for a given blade passage. The corresponding perturbation flow solution in each passage will also be harmonic of the form

$$\mathbf{U}_n^{jk}(\mathbf{x}, t) = \tilde{\mathbf{U}}_{jk}(\mathbf{x}) e^{i\omega_k t} e^{i(n-1)\sigma_j}, \quad (15)$$

where the vector  $\mathbf{U}_n$  represents the unknown perturbation flow variables associated with blade  $n$ . Thus if the response of the first blade ( $n = 1$ ) is known, the response of all subsequent blades can be determined by using (15). Therefore we solve the linearized Euler equations (7) in the first blade passage only, casting them in the frequency domain as

$$[i\omega_k - A_j] \tilde{\mathbf{U}}_{jk} = \mathbf{B} \tilde{\mathbf{u}}_{jk} + E \tilde{\mathbf{d}}_{jk}, \quad (16)$$

where  $A_j$  represents the the original matrix  $A$  in equation (7) modified to to impose complex periodicity of the solution; i.e. the solution must be identical if phase shifted by the interblade phase angle  $\sigma_j$ . Solutions of the frequency domain CFD equations (16) provide images of the unsteady flow field at each temporal frequency  $\omega_k$ , for each spatial frequency  $\sigma_j$ . The real and imaginary parts of these images form the snapshots for the projection analysis.

Although (16) implies that the snapshots are taken at imposed sinusoidal motions, as in assumed-frequency methods, this is merely a means of exciting the system dynamics to obtain a reduced-order subspace (next section). In the final projection step, all of the dynamics are projected onto this subspace, and a reduced-order model is obtained that is approximately valid for any general forcing function, provided its frequency content lies within the values of  $\omega_k$  sampled.

### Generation of an optimal set of basis vectors

To obtain the reduced-order model, the unknown flow solution vector is projected onto a small number of orthonormal basis functions  $\{\Psi_i\}$ , so that the flow dynamics can be represented as

$$\mathbf{U}'(t) = \sum_{i=1}^m v_i(t) \Psi_i. \quad (17)$$

If the basis set is chosen to be efficient, it can accurately represent the flow dynamics even though  $m$  is small. The following subsections outline two alternative methods to create the basis set.

**Proper Orthogonal Decomposition** The POD computes a basis set by seeking functions which optimally represent the flow solution  $\mathbf{U}'(t)$ . More specifically, they maximize the following cost (Sirovich, 1987):

$$\max_{\Phi} \frac{\langle |(\mathbf{U}', \Phi)|^2 \rangle}{\langle \Phi, \Phi \rangle} = \frac{\langle |(\mathbf{U}', \Psi)|^2 \rangle}{\langle \Psi, \Psi \rangle}, \quad (18)$$

where  $(\mathbf{U}', \Psi)$  denotes the inner product of the basis vector with the field  $\mathbf{U}'(t)$  and  $\langle \cdot \rangle$  represents a time-averaging operation. It can be shown that a necessary condition for (18) to hold is that  $\Psi$  is an eigenfunction of the kernel  $K$  defined by

$$K(\mathbf{x}, \mathbf{x}') = \frac{1}{n} \sum_{i=1}^n \mathbf{U}_i(\mathbf{x}) \mathbf{U}_i(\mathbf{x}'), \quad (19)$$

where  $\mathbf{U}_i(\mathbf{x})$  is the instantaneous perturbation flow field or snapshot at a frequency  $\omega_i$ , and the number of snapshots  $n$  is sufficiently large (Berkooz et al., 1993). The eigenvectors of  $K$  are of the form

$$\Psi = \sum_{i=1}^n B_i \mathbf{U}_i, \quad (20)$$

where  $B_i$  have been shown to be the eigenvectors of the eigenvalue decomposition of the correlation matrix  $C$ :

$$CB = \Lambda B \quad (21)$$

where the correlation matrix  $C$  is given by

$$C_{ij} = \frac{1}{n} (\mathbf{U}_i, \mathbf{U}_j). \quad (22)$$

The function that achieves the maximum in (18) corresponds to  $\lambda_1$ , the largest eigenvalue of  $C$  (Berkooz et al., 1993), and is constructed using the eigenvector associated with  $\lambda_1$  via the equation  $\Psi_1 = \sum_{j=1}^n \beta_j^1 \mathbf{U}_j$ , where  $B_i = [\beta_1^i \ \beta_2^i \ \dots \ \beta_n^i]$ . Subsequent functions correspond to the eigenvalues  $\lambda_i$  ordered according to size:  $\lambda_1 \geq \lambda_2 \geq \dots \geq \lambda_n$ . The subspace spanned by the resulting vectors  $\Psi_i$  minimizes the ‘‘averaged energy’’ or the 2-norm of the error between the exact and projected data.

**Arnoldi-based approach** An alternative approach for computing an efficient basis is to approximately match the transfer functions of the low-order system to those of the high-order system. The transfer function of the high-order system (7,8) for a single input  $u$  and single output  $y$  is

$$H(s) = \mathbf{c}(sI - A)^{-1} \mathbf{b}, \quad (23)$$

which can also be represented as a rational function

$$H(s) = \frac{N(s)}{D(s)}, \quad (24)$$

where the numerator  $N(s)$  and denominator  $D(s)$  are both polynomials in  $s$ . A  $q$ th order Padé approximation to the transfer function is defined as

$$H_q(s) = \frac{b_{q-1}s^{q-1} + \dots + b_1s + b_0}{a_qs^q + a_{q-1}s^{q-1} + \dots + a_1s + 1}, \quad (25)$$

where the  $2q$  coefficients  $a_j, b_j$ , are selected to match the first  $2q$  terms in a McLaurin expansion of the transfer function (23), written

$$H(s) = - \sum_{k=1}^{\infty} m_k s^k \quad (26)$$

where

$$m_k = \mathbf{c}^T A^{-(k+1)} \mathbf{b} \quad (27)$$

is called the  $k$ th moment of  $H(s)$ . The  $q$ th order Padé approximation (25) can be constructed via the Lanczos process and will match the first  $2q$  moments of  $H(s)$  (Feldmann and Freund, 1995). However this process carries with it no guarantees concerning the stability properties of the approximation.

Another option is to use the Arnoldi method to generate a set of vectors which spans the  $q$ th order Krylov subspace defined by

$$K_q(A, \mathbf{b}) = \text{span}\{A^{-1}\mathbf{b}, A^{-2}\mathbf{b}, \dots, A^{-q}\mathbf{b}\}. \quad (28)$$

This set of  $q$  ‘‘Arnoldi vectors’’ matches  $q$  moments of the system transfer function, only half the number matched by the Padé approximation. However, since the Arnoldi approach has the advantage of generating a congruent transformation, in many cases it generates models with guaranteed stability.

It is also possible to reduce systems with multiple inputs using the block Arnoldi method. For example, if we consider a system with two inputs  $u_1$  and  $u_2$ ,

$$\dot{\mathbf{U}}' = A\mathbf{U}' + \mathbf{b}_1 u_1 + \mathbf{b}_2 u_2, \quad (29)$$

then the block Arnoldi method is used to generate vectors which span the Krylov subspace

$$K_q(A, \mathbf{b}_1, \mathbf{b}_2) = \text{span}\{A^{-1}\mathbf{b}_1, A^{-1}\mathbf{b}_2, A^{-2}\mathbf{b}_1, A^{-2}\mathbf{b}_2, \dots, A^{-q}\mathbf{b}_1, A^{-q}\mathbf{b}_2\}. \quad (30)$$

We also note that it is not necessarily the first  $q$  moments which must be matched. If we were to consider a Taylor series expansion of the transfer function about some non-zero value of  $s$ , a model could be obtained which would give a better approximation of the system dynamics for higher frequencies. These multiple frequency point Arnoldi methods are described in Grimme (1997).

### Projection of equations onto optimal basis

Once the basis vectors  $\Psi_i$  have been computed, by whichever method chosen, the assumed expansion for the perturbation solution (17) is substituted into the governing equations (7). Making use of orthogonality, a system of ordinary differential equations for the modal coefficients is obtained as follows:

$$\frac{dv_i}{dt} = \Psi_i^T A \sum_{j=1}^m v_j \Psi_j + \Psi_i^T B \mathbf{u} + \Psi_i^T E \mathbf{d}. \quad (31)$$

Since solutions at different interblade phase angles are orthogonal to one another, the system of equations (31) can be constructed for each value of  $\sigma_j$  and combined to form a block diagonal state-space system for the entire bladed disk. For each pair of interblade phase angles  $\pm\sigma_j$ , a set of equations is obtained which has the following form:

$$\dot{\mathbf{v}}_{\sigma_j} = A_{\sigma_j} \mathbf{v}_{\sigma_j} + B_{\sigma_j} \mathbf{u}_{\sigma_j} + E_{\sigma_j} \mathbf{d}_{\sigma_j}. \quad (32)$$

In (32) the aerodynamic state and input vectors are given in interblade phase angle coordinates, whereas we require the blade motion to be expressed in blade coordinates for coupling with a structural model. Therefore we perform a transformation from traveling wave to standing wave coordinates as described in Dugundji and Bundas (1984), which can be written  $\mathbf{u}_{\sigma} = T \mathbf{u}$ . As a result, the block diagonal state-space matrix  $B_{\sigma}$  becomes block circulant. The final set of aerodynamic equations can then be written

$$\frac{d\mathbf{v}}{dt} = A \mathbf{v} + B_{\sigma} T \mathbf{u} + E \mathbf{d} \quad (33)$$

and

$$\mathbf{y} = C \mathbf{v}, \quad (34)$$

where  $\mathbf{v}$  contains the aerodynamic states for all interblade phase angles and the matrix  $A$  is block diagonal with the submatrices  $A_{\sigma_j}$ . The vector  $\mathbf{y}$  is any desired output, but for the problems considered here contains the forces and moments acting on the

blades, and outgoing perturbation waves at the passage inlet and exit.

Note that static corrections may be used to aid in capturing high-frequency dynamics as described in Romanowski and Dowell (1994). This was done for the POD model presented here. In this case the reduced-order model has a slightly different form. The static correction functions are particular solutions of the flow system and are precomputed by solving for steady flows with unit boundary conditions on blade position, velocity and external disturbance.